Dalton Transactions

Reactivity of Bi- and Monometallic Trifluoroacetates Towards Amorphous SiO_2

Journal:	*Dalton Transactions*
Manuscript ID	DT-ART-08-2022-002822.R1
Article Type:	Paper
Date Submitted by the Author:	02-Nov-2022
Complete List of Authors:	Munasinghe, Hashini; Wayne State University, Chemistry Imer, Marcos; Wayne State University, Chemistry Szlag, Regina; Wayne State University, Chemistry Suescun, Leopoldo; Universidad de la República, Facultad de Química Rabuffetti, Federico; Wayne State University, Chemistry

ARTICLE

Reactivity of Bi- and Monometallic Trifluoroacetates Towards Amorphous SiO_2

Received 00th January 20xx,
Accepted 00th January 20xx

DOI: 10.1039/x0xx00000x

Hashini N. Munasinghe,[a,⊥] Marcos R. Imer,[a,⊥] Regina G. Szlag,[a] Leopoldo Suescun,[b] and Federico A. Rabuffetti[a,†]

The reactivity of alkali–manganese(II) and alkali trifluoroacetates towards amorphous SiO_2 (a-SiO_2) was studied in the solid-state. $K_4Mn_2(tfa)_8$, $Cs_3Mn_2(tfa)_7(tfaH)$, $KH(tfa)_2$, and $CsH(tfa)_2$ (tfa = CF_3COO^-) were thermally decomposed under vacuum in fused quartz tubes. Three new bimetallic fluorotrifluoroacetates of formulas $K_4Mn_3(tfa)_9F$, $Cs_4Mn_3(tfa)_9F$, and $K_2Mn(tfa)_3F$ were discovered upon thermolysis at 175 °C. $K_4Mn_3(tfa)_9F$ and $Cs_4Mn_3(tfa)_9F$ feature a triangular-bridged metal cluster of formula $[Mn_3(\mu_3\text{-}F)(\mu_2\text{-}tfa)_6(tfa)_3]^{4-}$. In the case of $K_2Mn(tfa)_3F$, fluoride serves as an inverse coordination center for the tetrahedral metal cluster $K_2Mn_2(\mu_4\text{-}F)$. Fluorotrifluoroacetates may be regarded as intermediates in the transformation of bimetallic trifluoroacetates to fluoroperovskites $KMnF_3$, $CsMnF_3$, and Cs_2MnF_4, which crystallized between 250 and 600 °C. Decomposition of these trifluoroacetates also yielded alkali hexafluorosilicates K_2SiF_6 and Cs_2SiF_6 as a result of the fluorination of fused quartz. The ability to fluorinate fused quartz was observed for monometallic alkali trifluoroacetates as well. Hexafluorosilicates and heptafluorosilicates K_3SiF_7 and Cs_3SiF_7 were obtained upon thermolysis of $KH(tfa)_2$ and $CsH(tfa)_2$ between 200 and 400 °C. This ability was exploited to synthesize fluorosilicates under air by simply reacting alkali trifluoroacetates with a-SiO_2 powder.

Introduction

For a number of years our group has been working on the synthesis, crystal-chemistry, and reactivity of bimetallic trifluoroacetates.[1-5] We have established that the trifluoroacetato ligand (tfa = CF_3COO^-) can bridge atoms with dissimilar electronic and geometric requirements and that this ability can be exploited to synthesize bimetallic trifluoroacetates featuring alkali–manganese(II),[1, 5] alkaline-earth–manganese(II),[2] and alkali–alkaline-earth pairs.[4] $K_2Mn_2(tfa)_6(tfaH)_2(H_2O)$, $CsMn(tfa)_3$, $K_2Mn(tfa)_4$, $Cs_3Mn_2(tfa)_7(tfaH)$, $Ca_{3-x}Mn_x(tfa)_6(H_2O)_4$, and $RbCa(tfa)_3$ are some examples of this family of solid-state materials. These solids can be prepared as single-phase polycrystalline materials, which is advantageous to establish reactivity patterns. On this basis, we have extensively studied the thermal decomposition of bimetallic trifluoroacetates under inert atmosphere. Taking $K_2Mn_2(tfa)_6(tfaH)_2(H_2O)$ and $CsMn(tfa)_3$ as examples, we have demonstrated that these solids serve as self-fluorinating single-source precursors to the corresponding fluoroperovskites $KMnF_3$ and $CsMnF_3$.[1] Likewise, thermolysis of $K_2Mn(tfa)_4$ and $Cs_3Mn_2(tfa)_7(tfaH)$ provides synthetic access to layered fluoroperovskites K_2MnF_4 and Cs_2MnF_4, respectively.[5]

More recently, we began studying the thermal decomposition of bimetallic trifluoroacetates in fused quartz sealed tubes. Our main goal was to probe the ability of these solids to fluorinate amorphous SiO_2 (a-SiO_2), which could eventually open up a new solid-state route to ternary and quaternary fluorosilicates. Additionally, we sought to capture decomposition transients to shed light on the transformation of an organic–inorganic hybrid into a fully inorganic solid. Results from these studies are presented herein in two distinct sections. The first section is devoted to the thermolysis of bimetallic trifluoroacetates $K_2Mn(tfa)_4$ and $Cs_3Mn_2(tfa)_7(tfaH)$ in the 175–600 °C temperature range. Single-crystal and powder X-ray diffraction were used to identify thermal decomposition products; hexafluorosilicates K_2SiF_6 and Cs_2SiF_6 were among these products. This observation prompted us to investigate the reactivity of alkali trifluoroacetates $KH(tfa)_2$ and $CsH(tfa)_2$ towards a-SiO_2. We were motivated by the fact that, although alkali trifluoroacetates have been used as trifluoromethylating agents,[6-10] they have not been considered as reagents for the solid-state synthesis of fluorosilicates. Fluorosilicates M_2SiF_6 (M = Li–Cs) and M'_3SiF_7 (M′ = K–Cs) are extensively used as hosts for Mn^{4+} downconverting red phosphors.[11-19] Typically, these materials are synthesized through solution-phase routes that use aqueous HF as the fluorine source;[20] alternatively, HF is generated in situ by dissolving MHF_2 in H_3PO_4[21] or NH_4F in HCl.[15, 22] In either approach, the presence of HF imposes stringent requirements to synthetic procedures and equipment. Thus, the second section of this article focuses on probing the

[a] Department of Chemistry, Wayne State University, Detroit, MI 48202, USA.
[b] Cryssmat–Lab/DETEMA, Facultad de Química, Universidad de la República, Montevideo 11800, Uruguay.
⊥ These authors contributed equally.
† Corresponding author. Email: far@chem.wayne.edu

Electronic Supplementary Information (ESI) available: (1) thermal analyses of bimetallic trifluoroacetates, (2) crystal structures of bimetallic fluorotrifluoroacetates, (3) reflection list of Cs_2MnF_4, (4) crystal structure of $KH(tfa)_2$, and (5) control experiments using KF and CsF. See DOI: 10.1039/x0xx00000x.

reactivity of $KH(tfa)_2$ and $CsH(tfa)_2$ towards a-SiO_2; specifically, on their ability to act as mild fluorinating agents. $KH(tfa)_2$ and $CsH(tfa)_2$ were decomposed in fused quartz tubes at temperatures ranging between 200 and 400 °C. Thermolysis experiments were also carried out under air in the presence of commercially available a-SiO_2 powder. Powder X-ray diffraction was used to identify decomposition products. Results presented in this article are discussed from the standpoint of streamlining the solid-state synthesis of fluorosilicates.

Experimental

Synthesis of Bi- and Monometallic Trifluoroacetates. All experiments were carried out under nitrogen atmosphere using standard Schlenk techniques. K_2CO_3 (99%), Cs_2CO_3 (99.9%), $MnCO_3$ (99.9%), amorphous SiO_2 (99.8%, surface area 175–225 $m^2\ g^{-1}$), and anhydrous CF_3COOH (99%) were purchased from Sigma-Aldrich and used as received. Double-distilled water was used throughout. Polycrystalline bi- and monometallic trifluoroacetates were synthesized via solvent evaporation.[5, 23] The procedure for the preparation of phase-pure $K_4Mn_2(tfa)_8$ and $Cs_3Mn_2(tfa)_7(tfaH)$ is described in detail elsewhere.[5] Monometallic trifluoroacetates $KH(tfa)_2$ and $CsH(tfa)_2$ were synthesized by dissolving the corresponding metal carbonate (1 mmol) in a mixture of 3 mL of tfaH and 3 mL of double-distilled water in a 50 mL two-neck round-bottom flask. A colorless transparent solution was thus obtained. The flask containing the reaction mixture was immersed in a sand bath and solvent evaporation took place at 65 °C for 48 h under a constant flow of dry nitrogen (140 mL min^{-1}). The resulting white solids were stored in a nitrogen-filled glove box.

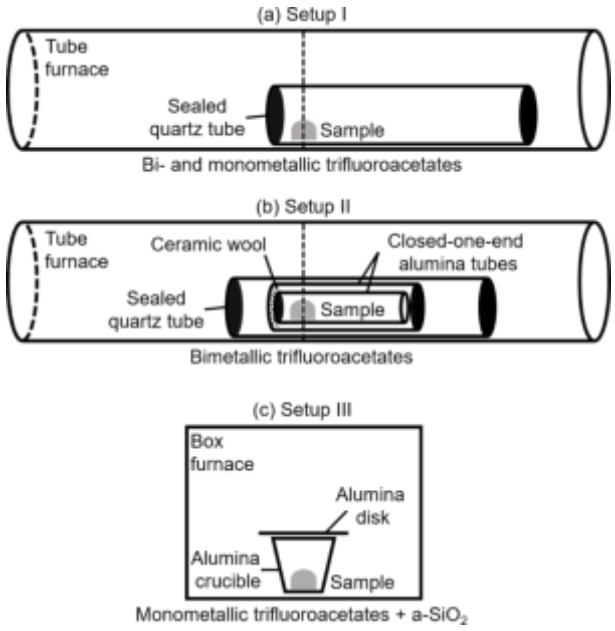

Figure 1. Experimental configurations used for thermolysis of bi- and monometallic trifluoroacetates. The tube furnace is 22 × 1′′ (length × diameter). The chamber of the box furnace is 4 × 5 × 7′′ (width × length × depth).

Thermal Decomposition of Trifluoroacetates. Thermolysis of trifluoroacetates was carried out in three different experimental configurations; these are depicted in Figure 1.

Setup I. Bimetallic (≈70–80 mg) and monometallic trifluoroacetates (≈120–150 mg) were first decomposed in setup I (Figure 1a). Polycrystalline samples were loaded into a fused quartz tube (length ≈120 mm, outer diameter ≈10 mm, wall thickness ≈1.0 mm). The tube was sealed under vacuum (≈45–60 mTorr), placed in a tube furnace at 100 °C, heated to a predefined target temperature (175–600 °C), and allowed to dwell at that temperature for a given time (2–12 h). A heating rate of 150 °C h^{-1} was employed in all cases except in experiments conducted at 175 °C, which were aimed at isolating single crystals of decomposition intermediates; in those experiments the heating rate was set to 6 °C h^{-1}. Once the dwelling time was completed, the furnace was allowed to cool to 100 °C, the quartz tube was opened under air, and products were stored in a nitrogen-filled glove box. Off-white to brown powders were obtained.

Setup II. Bimetallic trifluoroacetates (≈70–80 mg) were decomposed in setup II (Figure 1b). This experimental configuration differs from setup I in that the trifluoroacetate sample is not in direct contact with fused quartz. Polycrystalline samples were loaded into a closed-one-end alumina tube (length ≈70 mm, outer diameter ≈6.4 mm, wall thickness ≈1.0 mm). This tube was placed within a second alumina tube (length ≈70 mm, outer diameter ≈8.5 mm, wall thickness ≈1.0 mm). The open end of the tube containing the sample faced the closed end of the wider tube. Ceramic wool was used to fill the gap between the closed end of the tube containing the sample and the open end of the wider tube (≈2 mm). The whole assembly was placed in a fused quartz tube (length ≈120 mm, outer diameter ≈10 mm, wall thickness ≈1.0 mm) and sealed under vacuum (≈45–60 mTorr). Thermolysis was then carried out as in setup I. Off-white to brown powders were obtained.

Setup III. Monometallic trifluoroacetates were decomposed in setup III (Figure 1c). This experimental configuration differs from setups I and II in that (i) trifluoroacetates are decomposed in the presence of amorphous SiO_2 (alkali:Si molar ratio = 2:1), and (ii) thermolysis is carried out under air. $KH(tfa)_2$:a-SiO_2 (≈100 mg) and $CsH(tfa)_2$:a-SiO_2 (≈160 mg) mixtures were prepared in a nitrogen-filled glove box. These were transferred to 5 mL alumina crucibles, which were subsequently covered with alumina disks. Crucibles were placed in a box furnace at 100 °C, heated to a predefined target temperature (300–400 °C), and allowed to dwell at that temperature for a given time (6–12 h). A heating rate of 10 °C min^{-1} was employed in all experiments. Once the dwelling time was completed, the furnace was allowed to cool to 100 °C and crucibles were removed from the furnace. Ash grey powders were obtained. Dwelling temperatures were selected based on thermal analyses conducted under inert atmosphere which showed that $K_4Mn_2(tfa)_8$ and $Cs_3Mn_2(tfa)_7(tfaH)$ decompose between 150 and 275 °C (see **Figure S1** in the ESI and Figure 4 in reference 5). In the case of $KH(tfa)_2$ and $CsH(tfa)_2$, decomposition has been shown to take place between 150 and 250 °C.[24, 25]

Table 1. Crystal and Structural Determination Data of $K_4Mn_3(tfa)_9F$ and $K_2Mn(tfa)_3F$

Chemical formula	$K_4Mn_3(tfa)_9F$	$K_2Mn(tfa)_3F$
Formula weight (g)	1357.47	491.20
Crystal system	Monoclinic	Orthorhombic
Space group	$P2_1/n$	$Pbcn$
a, b, c (Å)	17.5481 (9), 13.7303 (7), 19.5024 (9)	12.4013 (10), 14.4480 (12), 7.3981 (6)
α, β, γ (°)	90, 109.993 (2), 90	90, 90, 90
Volume (Å^3)	4415.7 (4)	1325.55 (19)
Z	4	4
$R[F^2 > 2\sigma(F^2)]$	3.5%	10.3%
$wR(F^2)$	7.7%	25.2%
S	1.01	1.27

Single-Crystal X-ray Diffraction (SCXRD). SCXRD analysis was carried out to establish the crystal structures of intermediates formed upon thermolysis of $K_4Mn_2(tfa)_8$ and $Cs_3Mn_2(tfa)_7(tfaH)$ at 175 °C in setups I and II. Colorless crystals of $K_4Mn_3(tfa)_9F$ (0.48 × 0.32 × 0.25 mm), $Cs_4Mn_3(tfa)_9F$ (0.05 × 0.05 × 0.02 mm), and $K_2Mn(tfa)_3F$ (0.21 × 0.11 × 0.11 mm) were selected for structure determination and mounted in Paratone N oil. Diffraction data were collected using a Bruker X8 Apex diffractometer. X-ray intensities were measured at 100 K using Mo *K*α radiation (λ = 0.71073 Å). Frames were integrated using Bruker SAINT. Experimental data were corrected for Lorentz, polarization, and absorption effects; for the latter, the multiscan method was employed using Bruker SADABS.[26] Structure solution was accomplished using a dual-space approach as implemented in SHELXT[27] and difference Fourier maps as embedded in SHELXL-2014/7[28] running under ShelXle.[29] VESTA was used to visualize crystal structures.[30] **Table 1** summarizes crystal data for $K_4Mn_3(tfa)_9F$ and $K_2Mn(tfa)_3F$. $Cs_4Mn_3(tfa)_9F$ was found to be isostructural to its potassium counterpart, except for positional disorder of some cesium atoms and trifluoroacetate ligands. Full details on data collection and structure refinement are given in the ESI (**Tables S1–S10** and **Figures S2–S4**). Crystal data were deposited in the Cambridge Crystallographic Data Centre with numbers 2184179 ($K_4Mn_3(tfa)_9F$), 2201197 ($Cs_4Mn_3(tfa)_9F$), and 2184129 ($K_2Mn(tfa)_3F$).

Powder X-ray Diffraction (PXRD). Powder XRD patterns were collected using a Bruker D2Phaser diffractometer operated at 30 kV and 10 mA. Cu *Kα* radiation (λ = 1.5418 Å) was employed. A nickel filter was used to remove Cu Kβ. Diffractograms were collected in the 10–60° 2θ range using a step size of 0.012° and a step time of 0.4 s, unless otherwise noted.

Results and Discussion

Section I. Reactivity of Bimetallic Trifluoroacetates $K_4Mn_2(tfa)_8$ and $Cs_3Mn_2(tfa)_7(tfaH)$. Bimetallic trifluoroacetates $K_4Mn_2(tfa)_8$ and $Cs_3Mn_2(tfa)_7(tfaH)$ were thermally decomposed at 175, 250, 450, and 600 °C for 2 h in setups I and II. Crystalline phases obtained after each thermolysis experiment are summarized in **Table 2**. We begin our discussion of these results with the crystal structures of $K_4Mn_3(tfa)_9F$ and $K_2Mn(tfa)_3F$, which were obtained at 175 °C in setups I and II, respectively. Crystal structures are shown in **Figure 2**. $K_4Mn_3(tfa)_9F$ crystallizes in the monoclinic $P2_1/n$ space group and its building block consists of chains featuring corner-, edge-, and face-sharing MnO_5F and $K(O,F)_{10,11}$ polyhedra (**Figure 2a**). These chains run along the *c* axis and form layers that extend in the *bc* plane (**Figure 2b**). Stacking these layers along the *a* axis results in the observed three-dimensional structure in which each chain is connected to three adjacent chains (**Figure 2c**). An interesting structural feature of $K_4Mn_3(tfa)_9F$ is the presence of a triangular-bridged cluster of Mn^{2+} cations that may be described as $[Mn_3(\mu_3\text{-}F)(\mu_2\text{-}tfa)_6(tfa)_3]^{4-}$ (**Figure 2d**). A fluoride ion connects three MnO_5F octahedra by bridging Mn^{2+} in a trigonal planar geometry ($\angle Mn1–\mu_3\text{-}F–Mn2$ = 119.2°, $\angle Mn2–\mu_3\text{-}F–Mn3$ = 122.1°, $\angle Mn3–\mu_3\text{-}F–Mn1$ = 118.7°, Mn–F = 2.11–2.13 Å). Six trifluoroacetato ligands sitting above and below the plane of the $Mn_3(\mu_3\text{-}F)$ core bridge metal ions in pairs. The remaining three trifluoroacetato ligands complete the coordination sphere of manganese. The $[Mn_3(\mu_3\text{-}F)(\mu_2\text{-}tfa)_6(tfa)_3]^{4-}$ cluster was also encountered in

Table 2. Crystalline Products of the Solid-State Thermolysis of Bimetallic Trifluoroacetates

Precursor	Setup	Dwelling Temperature and Time			
		175 °C, 2 h	250 °C, 2 h	450 °C, 2 h	600 °C, 2 h
$K_4Mn_2(tfa)_8$	I	$K_4Mn_3(tfa)_9F$	$KMnF_3$	$KMnF_3$ K_2SiF_6 Unindexed phase(s)	$KMnF_3$ K_2SiF_6
	II	$K_2Mn(tfa)_3F$	$KMnF_3$	$KMnF_3$ K_2SiF_6	$KMnF_3$ K_2SiF_6
$Cs_3Mn_2(tfa)_7(tfaH)$	I	$Cs_4Mn_3(tfa)_9F$	$CsMnF_3$ Cs_2MnF_4 Cs_2SiF_6	Cs_2SiF_6 MnF_2	Cs_2SiF_6 MnF_2
	II	$Cs_4Mn_3(tfa)_9F$	$CsMnF_3$ Cs_2MnF_4 Cs_2SiF_6	$CsMnF_3$ Cs_2SiF_6 MnF_2	$CsMnF_3$ Cs_2SiF_6

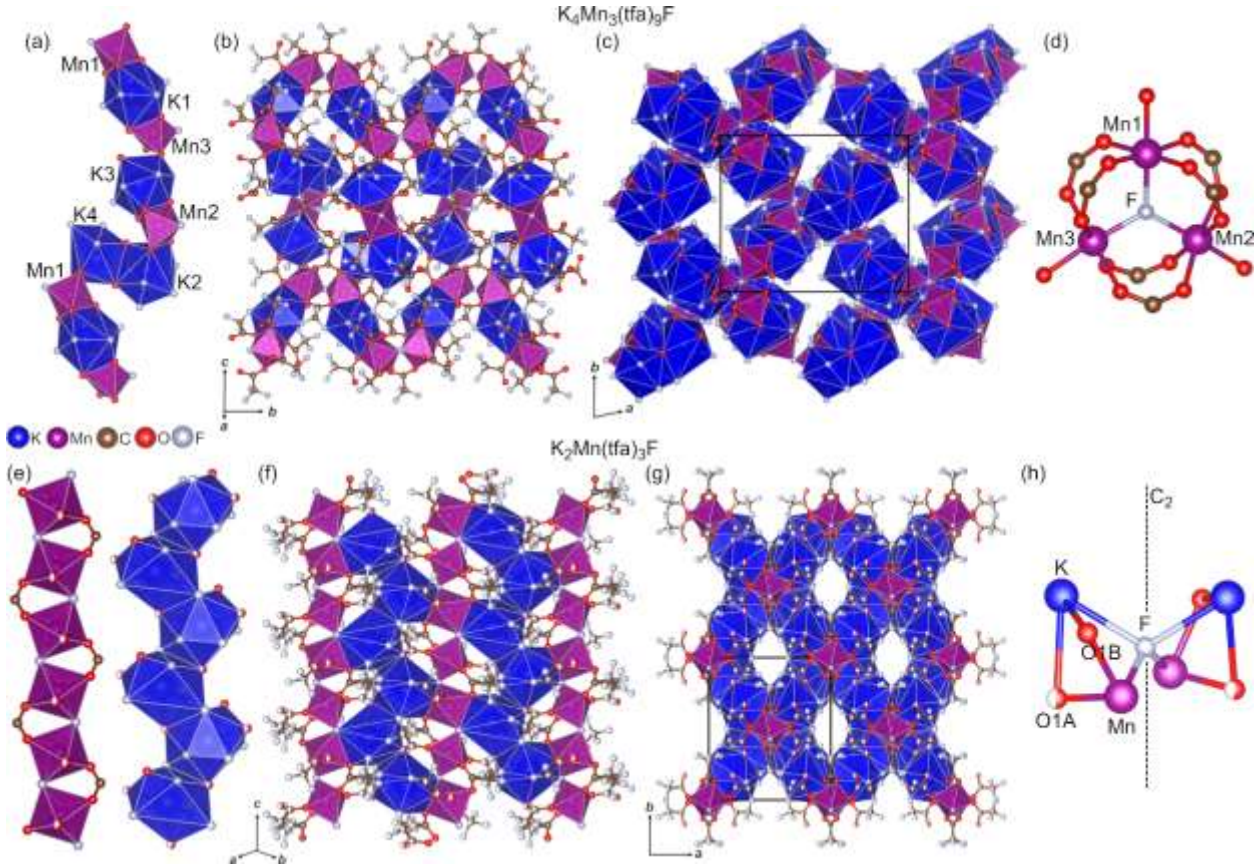

Figure 2. Crystal structures of $K_4Mn_3(tfa)_9F$ (a–d) and $K_2Mn(tfa)_3F$ (e–h). Building blocks (a, e), layers (b, f), and extended perspectives (c, g) are shown for each structure. (d) and (h) depict the coordination of bridging atoms μ_3-F and μ_4-F, respectively. Atom splitting in disordered positions is omitted for clarity; only major occupancy sites are shown. Unit cells in (c) and (g) are depicted with solid black lines. Only the polyhedral framework is shown in (c).

fluorotrifluoroacetates $Cs_4Mn_3(tfa)_9F$ and $Na_4Mn_3(tfa)_9F$, which are isostructural to $K_4Mn_3(tfa)_9F$. $Cs_4Mn_3(tfa)_9F$ was obtained upon thermal decomposition of $Cs_3Mn_2(tfa)_7(tfaH)$ at 175 °C. $Na_4Mn_3(tfa)_9F$ was synthesized in the course of exploratory thermolysis experiments conducted using a bimetallic sodium manganese trifluoroacetate previously reported by our group (see ESI, **Tables S11–S14** and **Figure S5**).[1] It is worth mentioning that triangular-bridged clusters of formula $M_3(\mu_3\text{-F})(tfa)_6L_3$ (M = Mg, Fe, Mn, Co, Ni, Zn; L = tfa, tfaH, OCH_3, py, H_2O) have been observed in fluorotrifluoroacetate crystals grown from solution at room temperature.[31-35] Altogether, these observations point to the relevance of these clusters as building blocks. Further, the fact that they are encountered both at room temperature and at 175 °C suggests their potential as synthons for the preparation of organic–inorganic hybrid materials. Another structurally interesting hybrid of formula $K_2Mn(tfa)_3F$ was discovered upon thermolysis of $K_4Mn_2(tfa)_8$ at 175 °C in setup II. $K_2Mn(tfa)_3F$ crystallizes in the orthorhombic *Pbcn* space group and can be visualized as chains built of corner-sharing MnO_4F_2 octahedra and edge-sharing $K(O,F)_{12}$ polyhedra (**Figure 2e**). These chains run along the *c* axis and are connected to each other through face-sharing polyhedra (**Figure 2f**). This connectivity results in layers that extend in the (110) and ($\bar{1}$10) planes. The observed three-dimensional structure of the hybrid results from the assembly of these two sets of layers (**Figure 2g**). Void channels that run parallel to the *c* axis are observed in $K_2Mn(tfa)_3F$; the presence of micropores in mono- and bimetallic haloacetates is not uncommon.[1, 23, 36, 37] An unusual structural motif we observe in $K_2Mn(tfa)_3F$ is a $K_2Mn_2(\mu_4\text{-F})$ cluster in which fluoride bridges two K^+ and two Mn^{2+} cations (**Figure 2h**). The bridging fluoride sits on a C_2 axis and the four metal ions are arranged in a highly distorted tetrahedral geometry ($\angle K\text{–}\mu_4\text{-F}\text{–}K = 116.9°$, $\angle Mn\text{–}\mu_4\text{-F}\text{–}Mn = 121.0°$, $\angle K\text{–}\mu_4\text{-F}\text{–}Mn = 94.1°$, K–F = 2.72 Å, Mn–F = 2.13 Å). Although μ_4-F is known to serve as an inverse coordination center in tetrahedral metal–organic complexes,[38] a comprehensive search shows that fluorotrifluoroacetates featuring μ_4-F metal clusters have not been reported neither in the literature nor in the *Cambridge Structural Database*. Attempts to isolate $Cs_2Mn(tfa)_3F$ by decomposing $Cs_3Mn_2(tfa)_7(tfaH)$ in setup II were unsuccessful; $Cs_4Mn_3(tfa)_9F$ was invariably obtained.

As shown in **Table 2** and as it will be discussed below, thermolysis of $K_4Mn_2(tfa)_8$ and $Cs_3Mn_2(tfa)_7(tfaH)$ at or above 250 °C led to the formation of fluoroperovskite phases $KMnF_3$, $CsMnF_3$, and Cs_2MnF_4. Fluorotrifluoroacetates $K_4Mn_3(tfa)_9F$, $Cs_4Mn_3(tfa)_9F$, and $K_2Mn(tfa)_3F$ isolated at 175 °C could therefore be regarded as intermediates in the transformation of bimetallic trifluoroacetates to fluoroperovskites. This conjecture results from compositional and structural considerations. From a compositional standpoint, organooxygen (from carboxylate groups) and organofluorine (from trifluoromethyl groups) are partially displaced from the

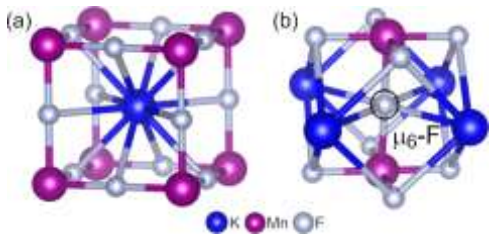

Figure 3. Crystal structure of cubic $KMnF_3$. Unit cell (a) and local coordination of the μ_6-F atom (b) are shown.

coordination sphere of metal atoms upon going from trifluoroacetates to fluorotrifluoroacetates. As an example, manganese atoms in $K_4Mn_2(tfa)_8$ are solely coordinated by organooxygen.[5] By contrast, MnO_5F and MnO_4F_2 octahedra present in $K_4Mn_3(tfa)_9F$ and $K_2Mn(tfa)_3F$, respectively, feature organooxygen and fluoride as ligands. The stepwise replacement of trifluoroacetato ligands by fluoride anions has been observed in the thermolysis of $Fe(tfa)_3$.[39] From a structural standpoint, the connectivity of metal atoms in $K_4Mn_3(tfa)_9F$ and $K_2Mn(tfa)_3F$ may be regarded as intermediate between that observed in bimetallic trifluoroacetates and fluoroperovskites. For clarity, the crystal structure of cubic $KMnF_3$ is shown in **Figure 3**. Continuing with the example of manganese atoms, no Mn–organofluorine–Mn bridges are present in $K_4Mn_2(tfa)_8$.[5] However, Mn–fluoride–Mn bridges are encountered in $K_4Mn_3(tfa)_9F$ and $K_2Mn(tfa)_3F$; these bridges build the framework of MnF_6 octahedra in $KMnF_3$ (**Figure 3a**). Additionally, K–fluoride–K and K–fluoride–Mn bridges are observed in the case of $K_2Mn(tfa)_3F$; such bridges are present in $KMnF_3$. From this perspective, the presence of a $K_2Mn_2(\mu_4\text{-F})$ cluster in $K_2Mn(tfa)_3F$ may be visualized as an intermediate towards the formation of the $K_4Mn_2(\mu_6\text{-F})$ core in $KMnF_3$ (**Figure 3b**). Similar compositional and structural relationships can be established between $Cs_3Mn_2(tfa)_7(tfaH)$, $Cs_4Mn_3(tfa)_9F$, hexagonal $CsMnF_3$, and tetragonal Cs_2MnF_4.

$K_4Mn_2(tfa)_8$ and $Cs_3Mn_2(tfa)_7(tfaH)$ were also decomposed at 250, 450, and 600 °C for 2 h in setups I and II. PXRD patterns of the decomposition products are given in **Figures 4** and **5**. Thermolysis of $K_4Mn_2(tfa)_8$ at 250 °C in setup I led to cubic $KMnF_3$ (PDF No. 01–073–9430) as the sole crystalline product (**Figure 4a**). The formation of K_2SiF_6 (PDF No. 01–075–0694) was observed upon increasing the decomposition temperature to 450 °C while keeping the dwelling time constant. Under these conditions, $KMnF_3$ and K_2SiF_6 coexisted with one or multiple crystalline phases (X) whose diffraction maxima could not be indexed (**Figure 4b**). Finally, only $KMnF_3$ and K_2SiF_6 were identified as crystalline products upon thermolysis at 600 °C (**Figure 4c**). Similar results were obtained in setup II except that (i) no crystalline phases other than $KMnF_3$ and K_2SiF_6 were observed at 450 °C, and (ii) the fraction of K_2SiF_6 relative to $KMnF_3$ at 600 °C was significantly lower than that observed in setup I (**Figure 4d–f**). In the case of $Cs_3Mn_2(tfa)_7(tfaH)$, $CsMnF_3$ (PDF No. 01–075–

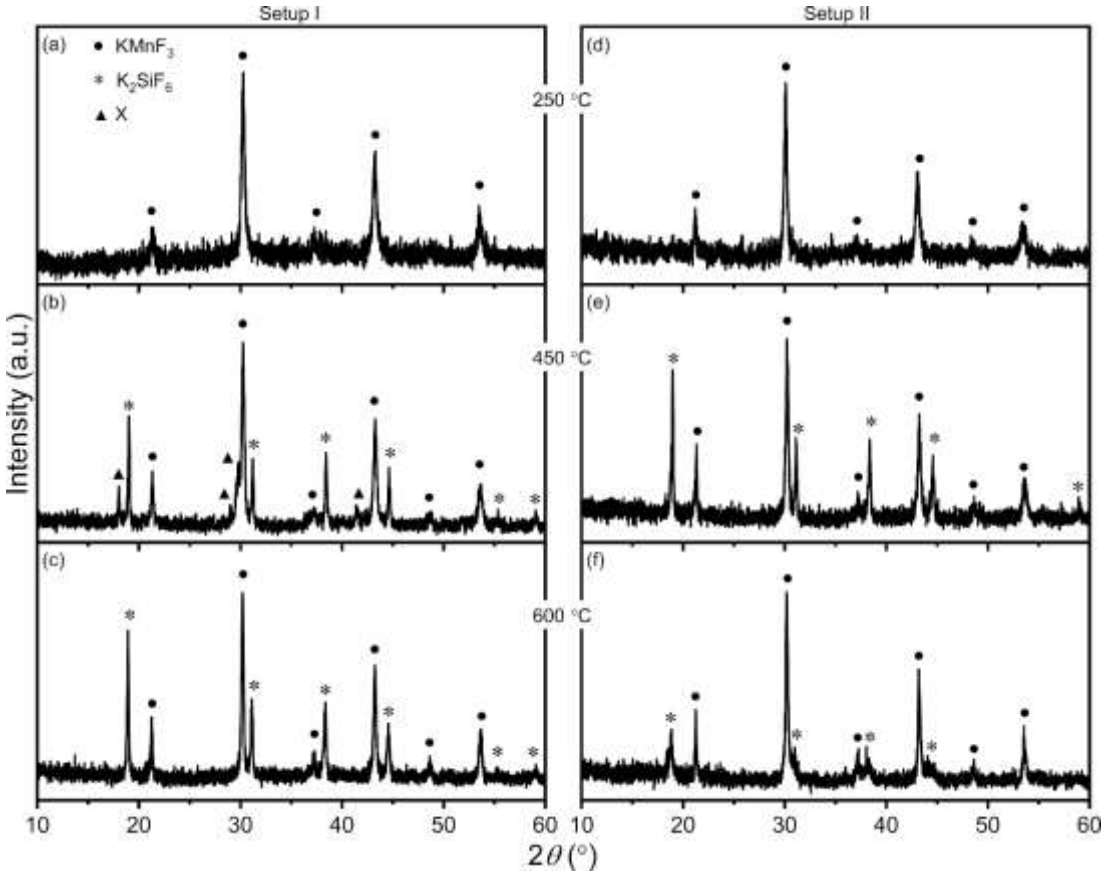

Figure 4. PXRD patterns of the products resulting from thermolysis of bimetallic trifluoroacetate $K_4Mn_2(tfa)_8$ in setups I (a–c) and II (d–f) at three different temperatures.

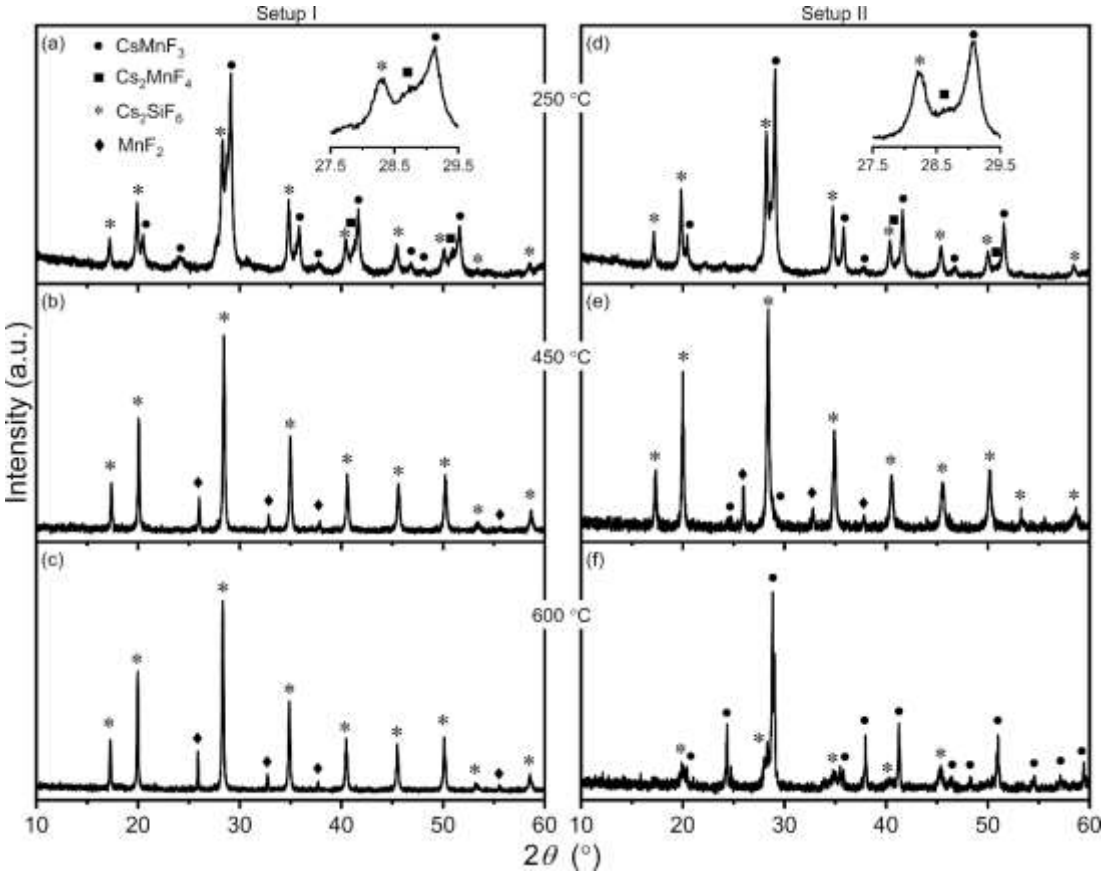

Figure 5. PXRD patterns of the products resulting from thermolysis of bimetallic trifluoroacetate $Cs_3Mn_2(tfa)_7(tfaH)$ in setups I (a–c) and II (d–f) at three different temperatures. Patterns shown in (a) and (d) were collected with a step time of 1.4 s.

2034), Cs_2MnF_4, and Cs_2SiF_6 (PDF No. 01–073–6564) were observed as crystalline products upon decomposition at 250 °C in setup I (**Figure 5a**). A tentative crystal structure of layered perovskite Cs_2MnF_4 was proposed by us in a recent article;[5] the corresponding reflection list is given in the ESI (**Table S15**). The hygroscopic nature of this phase complicated collection and indexing of diffraction data;[5] as a result, the presence of trace amounts of additional phases cannot be discarded. Increasing the decomposition temperature from 250 to 450 °C while keeping the dwelling time constant yielded Cs_2SiF_6 and MnF_2 (PDF No. 01–070–2499) as products (**Figure 5b**); $CsMnF_3$ was not observed under these conditions. Further increasing the temperature to 600 °C did not result in significant changes (**Figure 5c**). Similar results were obtained at 250 and 450 °C in setup II, except that for the latter temperature a very small fraction of hexagonal $CsMnF_3$ coexisted with Cs_2SiF_6 and MnF_2 (**Figure 5d** and **5e**). At 600 °C, by contrast, hexagonal $CsMnF_3$ was the major phase and coexisted with a minor fraction of Cs_2SiF_6; no MnF_2 was observed under these conditions (**Figure 5f**). As mentioned in the Introduction, our goal was to establish reactivity patterns towards a-SiO_2. Results presented in this paragraph, however, provide a starting point to formulate some hypotheses for future mechanistic studies aimed at elucidating fluorinating species, reaction pathways, and transients. The formation of alkali hexafluorosilicates was observed for both compounds and in both setups, implying that byproducts from trifluoroacetate thermolysis reacted with the quartz tube (or with the ceramic wool, which contains a-SiO_2) to form a silicon-containing gas such as SiF_4. Two pathways may be envisioned for the formation of this species. The first pathway involves fluorination of a-SiO_2 by difluorocarbene (equation (1));[40, 41] CF_2 has been proposed as a byproduct of trifluoroacetate thermolysis.[4, 42, 43] The second pathway involves etching of a-SiO_2 by gaseous hydrogen fluoride (equation (2)).[44, 45] HF may be formed upon hydrolysis of trifluoroacetic anhydride.

$$\text{a-SiO}_2 + 2CF_2 \rightarrow SiF_4 + 2CO \quad (1)$$

$$\text{a-SiO}_2 + 4HF \rightarrow SiF_4 + 2H_2O \quad (2)$$

$(CF_3CO)_2O$ has been identified as a byproduct of trifluoroacetate thermolysis[4, 43, 46-48] and the presence of residual water cannot be ruled out under our experimental conditions. Both fluorination pathways may be operating if water is present since hydrolysis of $(CF_3CO)_2O$ leads to the formation of trifluoroacetic acid which in turns produces difluorocarbene.[44, 45] Another result that deserves further investigation is whether alkali hexafluorosilicates form through reaction of fluoroperovskites with SiF_4. The presence of MnF_2 following the decomposition of $Cs_3Mn_2(tfa)_7(tfaH)$ suggests this reaction may be

$$2CsMnF_3 + SiF_4 \leftrightharpoons Cs_2SiF_6 + 2MnF_2 \quad (3)$$

Table 3. Crystalline Products of the Solid-State Thermolysis of Monometallic Trifluoroacetates[a]

Precursor	Setup	Dwelling Temperature and Time		
		200 °C, 12 h	300 °C, 12 h	400 °C, 12 h
$KH(tfa)_2$	I	K_2SiF_6	K_2SiF_6 K_3SiF_7	K_3SiF_7
	III		K_2SiF_6 K_3SiF_7	K_2SiF_6 K_3SiF_7
			300 °C, 6 h	400 °C, 6 h
$CsH(tfa)_2$	I		Cs_2SiF_6 Cs_3SiF_7	Cs_2SiF_6
	III			Cs_2SiF_6 Cs_3SiF_7

[a] Under a relative humidity of 20–25%.

occurring (equation (3)). At the same time, the fact that MnF_2 was not detected in the decomposition of $K_4Mn_2(tfa)_8$ raises the question of the dependence of the mechanism by which alkali hexafluorosilicates form on the alkali metal. Hypotheses regarding reaction pathways and transients should be considered with the caveat that decomposition reactions were not *sequential* because reaction mixtures were allowed to dwell for 2 h at each temperature. Future mechanistic studies should obviously employ a different experimental design.

Section II. Reactivity of Monometallic Trifluoroacetates $KH(tfa)_2$ and $CsH(tfa)_2$. The observation that bimetallic trifluoroacetates reacted with the quartz tube prompted us to investigate the reactivity of monometallic alkali trifluoroacetates $KH(tfa)_2$ and $CsH(tfa)_2$ towards a-SiO_2. Specifically, we were interested in establishing whether these solids could be used as reagents for the solid-state synthesis of fluorosilicates. $KH(tfa)_2$ and $CsH(tfa)_2$ crystallize in the monoclinic space group *C*2/*c* and are isostructural (see ESI, **Tables S16–S19** and **Figures S6** and **S7**).[49] These solids were decomposed in setups I and III to probe their reactivity towards a-SiO_2 first in vacuum and then under air. Thermal decomposition was carried out at temperatures between 200

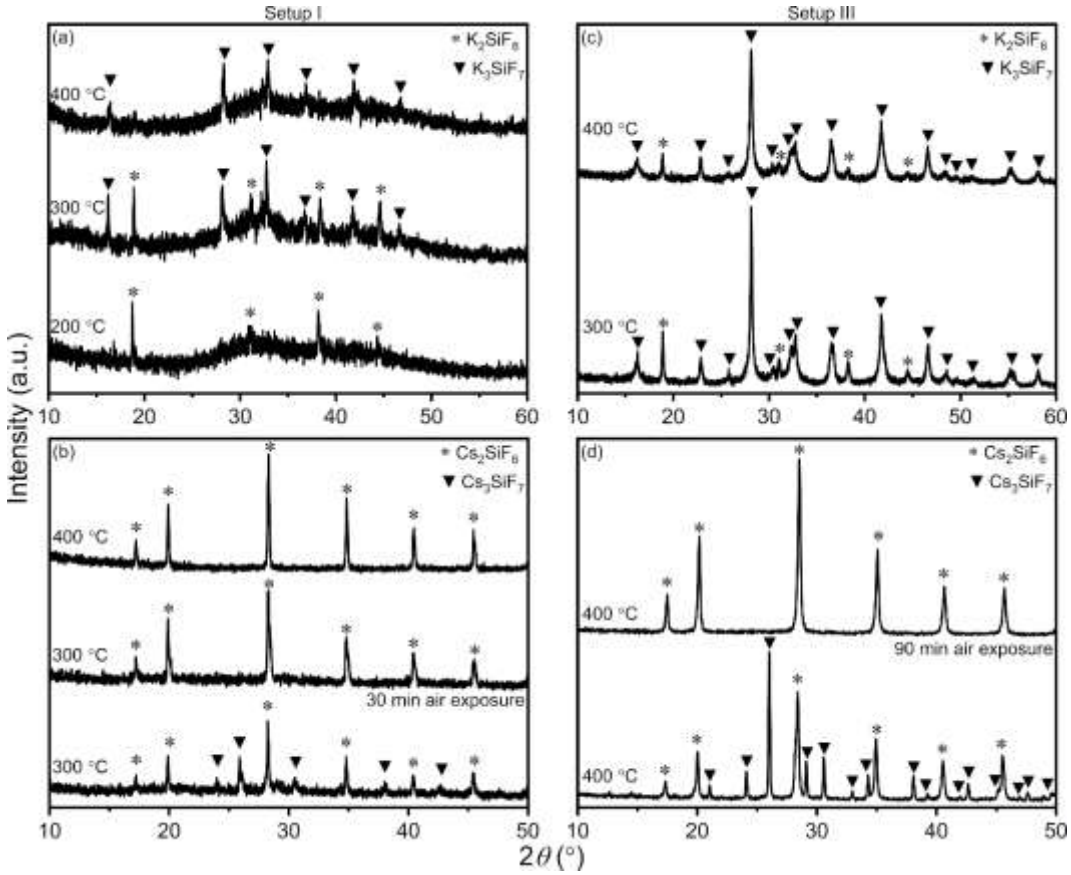

Figure 6. PXRD patterns of the products resulting from thermolysis of monometallic trifluoroacetates $KH(tfa)_2$ and $CsH(tfa)_2$ in setups I (a, b) and III (c, d).

and 400 °C for 6 to 12 h. Crystalline phases obtained after each thermolysis experiment are summarized in **Table 3**. PXRD patterns of the decomposition products are given in **Figure 6**. Owing to the hygroscopic nature of some of the products, diffraction patterns were collected immediately after opening the quartz tube (setup I) or after removing the alumina crucible from the box furnace (setup III), unless noted otherwise. Thermolysis of $KH(tfa)_2$ at 200 °C for 12 h in a sealed quartz tube resulted in the formation of K_2SiF_6 (PDF No. 01–075–0694) as the sole crystalline product (**Figure 6a**). Increasing the decomposition temperature to 300 °C led to the appearance of K_3SiF_7 (PDF No. 01–073–1396); at 400 °C, this was the only crystalline phase observed. As expected, increasing temperature stabilized K_3SiF_7 relative to K_2SiF_6.[50-52] Analysis of the decomposition products of $CsH(tfa)_2$ was significantly more challenging due to the extremely hygroscopic nature of Cs_3SiF_7.[53] Unlike K_3SiF_7, which decomposed after several hours under our experimental conditions (≈20–25% relative humidity), Cs_3SiF_7 decomposed within minutes. X-ray analysis of the products resulting from thermolysis of $CsH(tfa)_2$ at 200 °C for 6 h was not possible because the powder turned into a liquid right after opening the quartz tube. Increasing the decomposition temperature to 300 °C allowed us to observe the coexistence of Cs_2SiF_6 (PDF No. 01–073–6564) and Cs_3SiF_7 (PDF No. 01–071–0997, **Figure 6b**). Collection of a diffraction pattern of the same sample after 30 min of air exposure showed that Cs_3SiF_7 had already decomposed, leaving Cs_2SiF_6 as the only crystalline phase. Only maxima arising from Cs_2SiF_6 were observed in the products obtained upon thermolysis at 400 °C. Altogether, results from thermolysis experiments conducted in setup I established the ability of $KH(tfa)_2$ and $CsH(tfa)_2$ to fluorinate quartz under vacuum and yield ternary fluorosilicates. We then decided to probe whether this reactivity pattern was maintained under air. To this end, mixtures of $KH(tfa)_2$:a-SiO_2 and $CsH(tfa)_2$:a-SiO_2 (2:1 molar ratio) were decomposed in setup III. Thermolysis of $KH(tfa)_2$ was carried out at 300 and 400 °C for 12 h. Both K_2SiF_6 and K_3SiF_7 could be accessed in this temperature range (**Figure 6c**). $CsH(tfa)_2$ was decomposed at 400 °C for 6 h in an attempt to obtain phase pure Cs_2SiF_6. However, a mixture of Cs_2SiF_6 and Cs_3SiF_7 was obtained (**Figure 6d**); as expected, the latter phase decomposed within minutes. The most significant outcome of these experiments was that alkali trifluoroacetates were able to fluorinate a-SiO_2 in an experimental setup similar to that used for routine solid-state reactions. Further, control experiments performed in setup III using KF as a reagent showed that no reaction occurred with a-SiO_2 (see ESI, **Figure S8a**). Likewise, CsF was much less reactive towards a-SiO_2 than its trifluoroacetate counterpart (see ESI, **Figure S8b**), demonstrating that the strong fluorinating ability of $KH(tfa)_2$ and $CsH(tfa)_2$ stems from the trifluoroacetato ligands. This distinct reactivity of alkali trifluoroacetates could be exploited to design all-solid-state routes to alkali fluorosilicates as an alternative to currently used solution-based syntheses, which typically entail using aqueous HF.[20, 54] Tuning the stoichiometry of the reaction mixture and reaction conditions (mass, heating rate, and dwelling temperature and time) should enable the preparation of single-phase fluorosilicates using trifluoroacetates as a metal and fluorine source.

Conclusions

The reactivity of alkali–manganese(II) and alkali trifluoroacetates towards a-SiO_2 was probed in a number of experimental configurations. Three new bimetallic fluorotrifluoroacetates were discovered upon thermolysis of $K_4Mn_2(tfa)_8$ and $Cs_3Mn_2(tfa)_7(tfaH)$ under vacuum. $K_4Mn_3(tfa)_9F$, $Cs_4Mn_3(tfa)_9F$, and $K_2Mn(tfa)_3F$ may be regarded as intermediates in the transformation of the bimetallic trifluoroacetates to ternary fluoroperovskites. Decomposition of bimetallic trifluoroacetates also yielded alkali hexafluorosilicates K_2SiF_6 and Cs_2SiF_6 as a result of the fluorination of a-SiO_2. This reactivity pattern was exploited to create a straightforward all-solid-state route to hexa- and heptafluorosilicates via thermal decomposition of monometallic trifluoroacetates $KH(tfa)_2$ and $CsH(tfa)_2$ under air. These findings enlarge the library of fluorinated organic–inorganic hybrid materials and the toolbox of synthetic routes to fluorosilicates.

Future research avenues include (1) expanding the proposed solid-state route to more compositionally complex targets such as quaternary fluorosilicates,[55] (2) developing the chemistry to incorporate optically relevant dopants such as Mn^{4+} during the thermal decomposition stage, and (3) understanding the mechanistic aspects of the formation of fluorosilicates from metal trifluoroacetates (i.e., fluorinating species, phase equilibria, and kinetics).

Conflicts of interest

There are no conflicts to declare.

Acknowledgements

The authors would like to acknowledge the financial support of the National Science Foundation (DMR−2003118) and of the Michigan Space Grant Consortium (Grant NNX15AJ20H). They are also grateful for the support of Wayne State University through a Thomas C. Rumble Graduate Fellowship and for the use of the X-ray core in the Lumigen Instrument Center (National Institutes of Health supplement grant 3R01EB027103–02S1 and National Science Foundation grant MRI–1427926).

Notes and references

1. Dhanapala, B. D.; Munasinghe, H. N.; Suescun, L.; Rabuffetti, F. A., Bimetallic Trifluoroacetates as Single-Source Precursors for Alkali–Manganese Fluoroperovskites. *Inorganic Chemistry* **2017,** 56, 13311–13320.
2. Dhanapala, B. D.; Mannino, N. A.; Mendoza, L. M.; Dissanayake, K. T.; Martin, P. D.; Suescun, L.; Rabuffetti, F. A., Synthesis of Bimetallic Trifluoroacetates Through a Crystallochemical Investigation of Their Monometallic Counterparts: The Case of

(A, A')$(CF_3COO)_2 \cdot nH_2O$ (A, A' = Mg, Ca, Sr, Ba, Mn). *Dalton Transactions* **2017,** 46, 1420–1430.
3. Munárriz, J.; Rabuffetti, F. A.; Contreras-García, J., Building Fluorinated Hybrid Crystals: Understanding the Role of Noncovalent Interactions. *Crystal Growth & Design* **2018,** 18, 6901–6910.
4. Szlag, R. G.; Suescun, L.; Dhanapala, B. D.; Rabuffetti, F. A., Rubidium–Alkaline-Earth Trifluoroacetate Hybrids as Self-Fluorinating Single-Source Precursors to Mixed-Metal Fluorides. *Inorganic Chemistry* **2019,** 58, 3041–3049.
5. Munasinghe, H. N.; Suescun, L.; Dhanapala, B. D.; Rabuffetti, F. A., Bimetallic Trifluoroacetates as Precursors to Layered Perovskites A_2MnF_4 (A = K, Rb, and Cs). *Inorganic Chemistry* **2020,** 59, 17268–17275.
6. Kiyohide, M.; Etsuko, T.; Midori, A.; Kiyosi, K., A Convenient Trifluoromethylation of Aromatic Halides with Sodium Trifluoroacetate. *Chemistry Letters* **1981,** 10, 1719–1720.
7. Chang, Y.; Cai, C., Sodium Trifluoroacetate: An Efficient Precursor for the Trifluoromethylation of Aldehydes. *Tetrahedron Letters* **2005,** 46, 3161–3164.
8. Chen, M.; Buchwald, S. L., Rapid and Efficient Trifluoromethylation of Aromatic and Heteroaromatic Compounds Using Potassium Trifluoroacetate Enabled by a Flow System. *Angewandte Chemie International Edition* **2013,** 52, 11628–11631.
9. Bogdanov, V. P.; Dmitrieva, V. A.; Ioutsi, V. A.; Belov, N. M.; Goryunkov, A. A., Alkali Metal Trifluoroacetates for the Nucleophilic Trifluoromethylation of Fullerenes. *Journal of Fluorine Chemistry* **2019,** 226, 109344.
10. Bogdanov, V. P.; Dmitrieva, V. A.; Rybalchenko, A. V.; Yankova, T. S.; Kosaya, M. P.; Romanova, N. A.; Belov, N. M.; Borisova, N. E.; Troyanov, S. I.; Goryunkov, A. A., Para-$C_{60}(CF_2)(CF_3)$R: A Family of Chiral Electron Accepting Compounds Accessible Through a Facile One-Pot Synthesis. *European Journal of Organic Chemistry* **2021,** 2021, 5147–5150.
11. Adachi, S.; Takahashi, T., Direct Synthesis and Properties of K_2SiF_6:Mn^{4+} Phosphor by Wet Chemical Etching of Si Wafer. *Journal of Applied Physics* **2008,** 104, 023512.
12. Adachi, S.; Abe, H.; Kasa, R.; Arai, T., Synthesis and Properties of Hetero-Dialkaline Hexafluorosilicate Red Phosphor $KNaSiF_6$:Mn^{4+}. *Journal of The Electrochemical Society* **2011,** 159, J34–J37.
13. Nguyen, H.-D.; Lin, C. C.; Fang, M.-H.; Liu, R.-S., Synthesis of Na_2SiF_6:Mn^{4+} Red Phosphors for White LED Applications by Co-Precipitation. *Journal of Materials Chemistry C* **2014,** 2, 10268–10272.
14. Jin, Y.; Fang, M.-H.; Grinberg, M.; Mahlik, S.; Lesniewski, T.; Brik, M. G.; Luo, G.-Y.; Lin, J. G.; Liu, R.-S., Narrow Red Emission Band Fluoride Phosphor $KNaSiF_6$:Mn^{4+} for Warm White Light-Emitting Diodes. *ACS Applied Materials & Interfaces* **2016,** 8, 11194–11203.
15. Luo, X.; Hou, Z.; Zhou, T.; Xie, R.-J., A Universal HF-Free Synthetic Method to Highly Efficient Narrow-Band Red-Emitting A_2XF_6:Mn^{4+} (A = K, Na, Rb, Cs; X = Si, Ge, Ti) Phosphors. *Journal of the American Ceramic Society* **2020,** 103, 1018–1026.
16. Zhong, X.; Deng, D.; Wang, T.; Li, Y.; Yu, Y.; Qiang, J.; Liao, S.; Huang, Y.; Long, J., High Water Resistance and Luminescent Thermal Stability of $Li_yNa_{(2-y)}SiF_6$:Mn^{4+} Red-Emitting Phosphor Induced by Codoping of Li^+. *Inorganic Chemistry* **2022,** 61, 5484–5494.
17. Kim, M.; Park, W. B.; Bang, B.; Kim, C. H.; Sohn, K.-S., A Novel Mn^{4+}-Activated Red Phosphor for Use in Light Emitting Diodes, K_3SiF_7:Mn^{4+}. *Journal of the American Ceramic Society* **2017,** 100, 1044–1050.
18. Kim, M.; Park, W. B.; Lee, J.-W.; Lee, J.; Kim, C. H.; Singh, S. P.; Sohn, K.-S., Rb_3SiF_7:Mn^{4+} and Rb_2CsSiF_7:Mn^{4+} Red-Emitting Phosphors with a Faster Decay Rate. *Chemistry of Materials* **2018,** 30, 6936–6944.
19. Jang, S.; Park, J. K.; Kim, M.; Sohn, K.-S.; Kim, C. H.; Chang, H., New Red-Emitting Phosphor $Rb_xK_{3-x}SiF_7$:Mn^{4+} (*x* = 0, 1, 2, 3): DFT Predictions and Synthesis. *RSC Advances* **2019,** 9, 39589–39594.
20. Kim, Y. H.; Ha, J.; Im, W. B., Towards Green Synthesis of Mn^{4+}-Doped Fluoride Phosphors: A Review. *Journal of Materials Research and Technology* **2021,** 11, 181–195.
21. Huang, L.; Zhu, Y.; Zhang, X.; Zou, R.; Pan, F.; Wang, J.; Wu, M., HF-Free Hydrothermal Route for Synthesis of Highly Efficient Narrow-Band Red Emitting Phosphor $K_2Si_{1-x}F_6$:xMn^{4+} for Warm White Light-Emitting Diodes. *Chemistry of Materials* **2016,** 28, 1495–1502.
22. Hou, Z.; Tang, X.; Luo, X.; Zhou, T.; Zhang, L.; Xie, R.-J., A Green Synthetic Route to the Highly Efficient K_2SiF_6:Mn^{4+} Narrow-Band Red Phosphor for Warm White Light-Emitting Diodes. *Journal of Materials Chemistry C* **2018,** 6, 2741–2746.
23. Dissanayake, K. T.; Mendoza, L. M.; Martin, P. D.; Suescun, L.; Rabuffetti, F. A., Open-Framework Structures of Anhydrous $Sr(CF_3COO)_2$ and $Ba(CF_3COO)_2$. *Inorganic Chemistry* **2016,** 55, 170–176.
24. Dallenbach, R.; Tissot, P., Properties of Molten Alkali Metal Trifluoroacetates. Part I. Study of the Binary System CF_3COOK–CF_3COONa. *Journal of Thermal Analysis* **1977,** 11, 61-69.
25. Dallenbach, R.; Tissot, P., Properties of Molten Alkali Metal Trifluoroacetates. Part II. Thermal Properties and Kinetics of Thermal Decomposition. *Journal of Thermal Analysis* **1981,** 20, 409–417.
26. Krause, L.; Herbst-Irmer, R.; Sheldrick, G. M.; Stalke, D., Comparison of Silver and Molybdenum Microfocus X-ray Sources for Single-Crystal Structure Determination. *Journal of Applied Crystallography* **2015,** 48, 3–10.
27. Sheldrick, G., Crystal Structure Refinement with SHELXL. *Acta Crystallographica Section C* **2015,** 71, 3–8.
28. Sheldrick, G. M. *SHELXL 2014/7: Program for Crystal Structure Solution*, University of Gottingen: 2014.
29. Hubschle, C. B.; Sheldrick, G. M.; Dittrich, B., ShelXle: a Qt Graphical User Interface for SHELXL. *Journal of Applied Crystallography* **2011,** 44, 1281–1284.
30. Momma, K.; Izumi, F., VESTA 3 for Three-Dimensional Visualization of Crystal, Volumetric and Morphology Data. *Journal of Applied Crystallography* **2011,** 44, 1272–1276.
31. Tereshchenko, D. S.; Morozov, I.; Boltalin, A. I.; Kemnitz, E.; Troyanov, S. I., Trinuclear Co(II) and Ni(II) Complexes with Tridentate Fluorine, $[M_3(\mu_3\text{-}F)(CF_3COO)_6(CF_3COOH)_3]^-$: Synthesis and Crystal Structure. *Zhurnal Neorganicheskoj Khimii* **2004,** 49, 919–928.
32. Noack, J.; Fritz, C.; Flügel, C.; Hemmann, F.; Gläsel, H.-J.; Kahle, O.; Dreyer, C.; Bauer, M.; Kemnitz, E., Metal Fluoride-Based Transparent Nanocomposites with Low Refractive Indices. *Dalton Transactions* **2013,** 42, 5706–5710.
33. Tereshchenko, D. S.; Morozov, I. V.; Boltalin, A. I.; Karpova, E. V.; Glazunova, T. Y.; Troyanov, S. I., Alkali Metal and Ammonium Fluoro(trifluoroacetato)metallates $M'[M''_3(\mu_3\text{-}F)(CF_3COO)_6(CF_3COOH)_3]$, where M' = Li, Na, K, NH_4, Rb, or Cs and M'' = Ni or Co. Synthesis and Crystal Structures. *Crystallography Reports* **2013,** 58, 68–77.
34. Morozov, I. V.; Karpova, E. V.; Glazunova, T. Y.; Boltalin, A. I.; Zakharov, M. A.; Tereshchenko, D. S.; Fedorova, A. A.; Troyanov, S. I., Trifluoroacetate Complexes of 3*d* Elements: Specific Features of Syntheses and Structures. *Russian Journal of Coordination Chemistry* **2016,** 42, 647–661.
35. Glazunova, T. Y.; Tereshchenko, D. S.; Buzoverov, M. E.; Karpova, E. V.; Lermontova, E. K., Synthesis and Crystal Structures of New Potassium Fluorotrifluoroacetatometallates: $K_n[M_3(\mu_3\text{-}F)(CF_3COO)_6L_3]L'$ (M = Co, Ni; L = CF_3COO^-, CF_3COOH, H_2O; L' = CF_3COOH, H_2O; *n* = 1, 2). *Russian Journal of Coordination Chemistry* **2021,** 47, 347–355.

36. Dissanayake, K. T.; Amarasinghe, D. K.; Suescun, L.; Rabuffetti, F. A., Accessing Mixed-Halide Upconverters Using Heterohaloacetate Precursors. *Chemistry of Materials* **2019,** 31, 6262–6267.
37. Dhanapala, B. D.; Munasinghe, H. N.; Dissanayake, K. T.; Suescun, L.; Rabuffetti, F. A., Expanding the Synthetic Toolbox to Access Pristine and Rare-Earth-Doped BaFBr Nanocrystals. *Dalton Transactions* **2021,** 50, 16092–16098.
38. Haiduc, I., Inverse Coordination – An Emerging New Chemical Concept. II. Halogens as Coordination Centers. *Coordination Chemistry Reviews* **2017,** 348, 71–91.
39. Wörle, M.; Guntlin, C. P.; Gyr, L.; Sougrati, M. T.; Lambert, C.-H.; Kravchyk, K. V.; Zenobi, R.; Kovalenko, M. V., Structural Evolution of Iron(III) Trifluoroacetate upon Thermal Decomposition: Chains, Layers, and Rings. *Chemistry of Materials* **2020,** 32, 2482–2488.
40. Birchall, J. M.; Haszeldine, R. N.; Roberts, D. W., Cyclopropane Chemistry. Part II. Cyclopropanes as Sources of Difluorocarbene. *Journal of the Chemical Society, Perkin Transactions 1* **1973**, 0, 1071–1078.
41. Barela, M. J.; Anderson, H. M.; Oehrlein, G. S., Role of C_2F_4, CF_2, and Ions in C_4F_8/Ar Plasma Discharges Under Active Oxide Etch Conditions in an Inductively Coupled GEC Cell Reactor. *Journal of Vacuum Science & Technology A* **2005,** 23, 408–416.
42. Farjas, J.; Camps, J.; Roura, P.; Ricart, S.; Puig, T.; Obradors, X., The Thermal Decomposition of Barium Trifluoroacetate. *Thermochimica Acta* **2012,** 544, 77–83.
43. Mosiadz, M.; Juda, K. L.; Hopkins, S. C.; Soloducho, J.; Glowacki, B. A., An In-Depth in situ IR Study of the Thermal Decomposition of Yttrium Trifluoroacetate Hydrate. *Journal of Thermal Analysis and Calorimetry* **2012,** 107, 681–691.
44. Blake, P. G.; Pritchard, H., The Thermal Decomposition of Trifluoroacetic Acid. *Journal of the Chemical Society B: Physical Organic* **1967**, 0, 282–286.
45. Jollie, D. M.; Harrison, P. G., An in situ IR Study of the Thermal Decomposition of Trifluoroacetic Acid. *Journal of the Chemical Society, Perkin Transactions 2* **1997**, 8, 1571–1576.
46. Rillings, K. W.; Roberts, J. E., A Thermal Study of the Trifluoroacetates and Pentafluoropropionates of Praseodymium, Samarium and Erbium. *Thermochimica Acta* **1974,** 10, 269–277.
47. Eloussifi, H.; Farjas, J.; Roura, P.; Camps, J.; Dammak, M.; Ricart, S.; Puig, T.; Obradors, X., Evolution of Yttrium Trifluoroacetate During Thermal Decomposition. *Journal of Thermal Analysis and Calorimetry* **2012,** 108, 589–596.
48. Opata, Y. A.; Grivel, J. C., Synthesis and Thermal Decomposition Study of Dysprosium Trifluoroacetate. *Journal of Analytical and Applied Pyrolysis* **2018,** 132, 40–46.
49. Golič, L.; Speakman, J. C., The Crystal Structures of the Acid Salts of Some Monobasic Acids. Part X. Potassium, Rubidium, and Cæsium Hydrogen Di-Trifluoroacetates. *Journal of the Chemical Society* **1965**, 0, 2530–2542.
50. Deadmore, D. L.; Bradley, W. F., The Crystal Structure of K_3SiF_7. *Acta Crystallographica* **1962,** 15, 186–189.
51. Kolditz, L.; Wilde, W.; Bentrup, U., Zur Bildung der Phase K_3SiF_7 Durch Thermische Zersetzung von $K_2[SiF_6]$. *Zeitschrift für Chemie* **1983,** 23, 246–247.
52. Vanetsev, A.; Põdder, P.; Oja, M.; Khaidukov, N. M.; Makhov, V. N.; Nagirnyi, V.; Romet, I.; Vielhauer, S.; Mändar, H.; Kirm, M., Microwave-Hydrothermal Synthesis and Investigation of Mn-Doped K_2SiF_6 Microsize Powder as a Red Phosphor for Warm White LEDs. *Journal of Luminescence* **2021,** 239, 118389.
53. Hofmann, B.; Hoppe, R., Zur Kenntnis des $(NH_4)_3SiF_7$-Typs. Neue Metallfluoride A_3MF_7 mit M = Si, Ti, Cr, Mn, Ni und A = Rb, Cs. *Zeitschrift für Anorganische und Allgemeine Chemie* **1979,** 458, 151–162.
54. Singh, V. S.; Moharil, S. V., Synthesis and Characterization of K_2SiF_6 Hexafluorosilicate. *IOP Conference Series: Materials Science and Engineering* **2021,** 1104, 012004.
55. Stoll, C.; Seibald, M.; Baumann, D.; Bandemehr, J.; Kraus, F.; Huppertz, H., $KLiSiF_6$ and $CsLiSiF_6$ – A Structure Investigation. *European Journal of Inorganic Chemistry* **2021,** 2021, 62–70.

Table of Contents

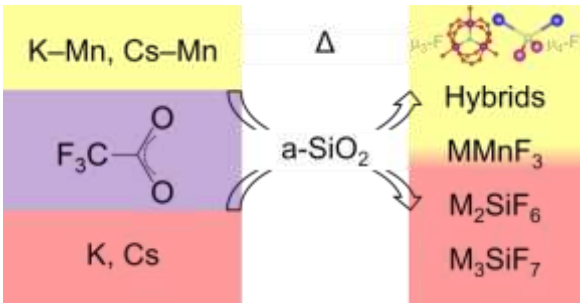

The reactivity of alkali–manganese(II) and alkali trifluoroacetates towards amorphous SiO_2 was studied in the solid-state with an eye towards the synthesis of alkali fluorosilicates.